Sensitivity Analysis and Tipping Calibration of A W-band Radiometer for Radiometric Measurements

Li Wu, Shusheng Peng, Zelong Xiao, and Jianzhong Xu

School of Electronic and Optical Engineering
Nanjing University of Science & Technology, Nanjing, 210094, China
li_wu@njust.edu.cn, pengshusheng@njust.edu.cn, zelongxiao@njust.edu.cn, xjz2018@yeah.net

Abstract ─ This paper deals with the sensitivity analysis and tipping calibration of a developed W-band radiometer system for radiometric measurements. Initially the equivalent integration time of the cascaded hardware and software integrators is derived and the radiometer sensitivity is then analyzed based on the established system measurement equation. Secondly, the applicable tipping calibration of the W-band radiometer is investigated and optimized to reduce calibration errors according to the system parameters. Sensitivity measurement and tipping calibration experiments of the developed W-band radiometer are conducted. The preliminary results show that the radiometer sensitivity is 0.51 K with an integration time of 1 s, and the tipping calibration has a better accuracy than the liquid nitrogen calibration, with a maximum difference of 2.5 K between both of the calibration methods.

Index Terms ─ Calibration, radiometric measurement, remote sensing, sensitivity.

I. INTRODUCTION

Due to the advantages of relatively simple design and high safety, radiometric sensors are increasingly being seen in non-invasive monitoring in harsh and or sensitive environments, such as the human body core where direct contact to the object under investigation is unachievable [1]. As lower microwave frequencies have penetration depths in tissues on the order of centimeters, microwave radiometric sensors have been employed to continuously monitor core body temperature which can provide a tool for monitoring drug delivery for cancer treatment [2], breast cancer detection [3], and hyperthermia temperature control [4,5]. While for the ingestible capsules which employs short-range wireless sensors to measure core body temperature [6], they measure the temperature somewhere in the digestive tract for a limited time and the device is still in the body.

At millimeter wave (MMW) frequencies, the penetration depth is limited to the top skin layer and can be used for surface temperature monitoring, such as in the case of surface burns [2]. Also, MMW radiometers are widely applied in security screening due to the advantage of clothes penetration. It is significant to accurately characterize the radiation of interested items like metal guns and knives, plastic explosives, ceramic knives to offer database for the detection, classification and identification [7].

A total power radiometer (TPR) for non-contact biomedical sensing is presented in [8] as a precursor to developing a health monitoring device. Unfortunately, the radiometer sensitivity, which is a critical issue in biomedical applications, is poor for the TPR due to system gain fluctuation. The Dicke radiometers are developed in [9,10] to stabilize the output for non-invasive temperature monitoring. However, any method that requires additional RF hardware will likely increase its system cost significantly [11]. Of all the approaches for radiometer sensitivity improvement, the noise-adding radiometer has the great potential to achieve this with minimal RF hardware added and has attracted a lot of attention [11-13]. Recently, a W-band radiometer which employs a receiver configuration based on the proposed radiometer in [13] was developed for radiometric characterization of interested items. It reduces the influences of unavoidable system gain fluctuations by injecting noise into the front end periodically. However, the sensitivity of the whole radiometer system was not presented in [13] which just analyzed the sensitivity of individual channels. And the both hardware and software integrators which contribute to the system integration time are employed for the flexibility in the receiver, so it is essential to derive the system sensitivity and the cascaded system integration time which determines the radiometer sensitivity directly.

Additionally, it is significant for an antenna to have a lower side-lobe level and a higher main-beam efficiency for radiometry. In this paper, an offset parabolic antenna is employed for the W-band radiometer to improve the measurement accuracy [14]. However, it is difficult to calibrate the developed radiometer with the offset parabolic antenna using the two point calibration method where a liquid nitrogen cooled absorber is

Submitted On: September 14, 2015
Accepted On: May 2, 2016

preferred in practical outdoor operations. Fortunately, the tipping calibration method which takes the atmosphere under clear weather conditions as a calibration reference is very convenient for the ground-based radiometer [15,16].

Aiming for the sensitivity analysis and the tipping calibration of the developed W-band radiometer with an offset parabolic antenna for radiometric measurements, this paper will be organized as follows. Section 2 introduces the developed radiometer receiver and establishes the corresponding system measurement model. The integration time of a cascaded integrator is derived and the sensitivity of the radiometer is analyzed in Section 3. The implementation of tipping calibration for the W-band radiometer and the primary calibration errors are described in Section 4. Experimental results and analysis are presented in Section 5. The last section is the conclusion.

II. THE DEVELOPED W-BAND RADIOMEER

Figure 1 shows the block diagram of an improved W-band radiometer receiver based on the noise adding type. While the radiometer working, the noise of antenna or matched load is added with the injected noise introduced by the noise source modulated with a periodic square wave. The coupled signal is converted to an IF signal via the mixer and goes through the IF amplifier, and the square law detector and is then divided into the direct current (DC) channel and the alternative current (AC) channel. Compared with the DC channel, the extra DC-block capacitor and the synchronous demodulator are needed for the AC channel. The output signals of the both channels are then acquired and processed by the data acquisition and processing unit to deduce the observed brightness temperature by applying the radiometer system measurement equations.

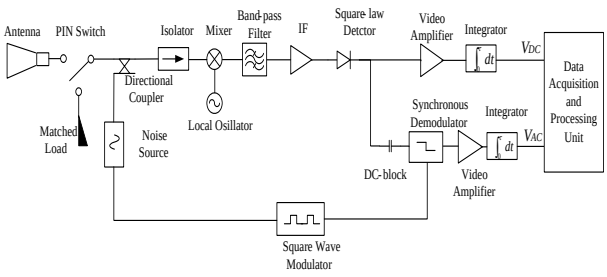

Fig. 1. Block diagram of the radiometer receiver.

The receiver front-end is housed in an insulated box with the stable temperature accomplished by a thermal controller. It is helpful to stabilize the receiver temperature due to the gain of the radiometer front-end is sensitive to the temperature variation. The W-band radiometer is placed on a two-dimensional scanner driven by a servo controller when it works. A picture of the W-band radiometer is shown in Fig. 2.

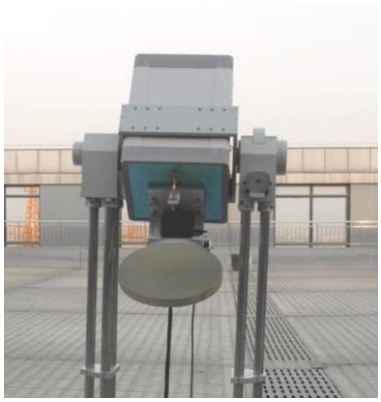

Fig. 2. A picture of the developed W-band radiometer.

When the PIN switch is connected to the antenna, the radiometer observes the scene to be measured. Suppose T_a is the antenna temperature, T_R is the equivalent system input noise temperature of the radiometer receiver, T_H and T_L are the noise temperatures injected into the coupler when the noise source is on and off, respectively. Then the radiometer system noise temperature with the noise source switched on and off can be respectively written as:

$$T_{s\_on} = T_a + T_R + T_H , \tag{1}$$

$$T_{s\_off} = T_a + T_R + T_L . \tag{2}$$

The difference between T_{s_on} and T_{s_off} is:

$$T_N = T_H - T_L = C_C \cdot T_o \cdot \mathrm{ENR} , \tag{3}$$

where C_c is the coupling factor of the coupler, T_o=290 K is the standard temperature, ENR is the excess noise ratio of the noise source. So the mean voltage components of DC channel and AC channel outputs can be expressed respectively as:

$$V_{DC} = \gamma_d G_c g_{dc} kB\left(T_s + T_{NM}\right), \tag{4}$$

$$V_{AC} = \gamma_d G_c g_{ac} kBT_{NM} , \tag{5}$$

where, V_{DC} and V_{AC} are the output voltages of DC channel and AC channel respectively, γ_d is the square-law detector sensitivity, G_c is the common receiver RF gain, g_{dc} and g_{ac} are the video amplifier gains of DC channel and AC channel respectively, k is the Boltzmann constant, B is the system bandwidth pre-detection, T_s is the receiver system noise temperature, and T_{NM}=T_N/2 is half of the injected noise temperature difference. Define a variable of K to be a ratio between the DC channel output voltage V_{DC} and the AC channel output voltage V_{AC}:

$$K = \frac{V_{DC}}{V_{AC}} = \frac{g_{dc}\left(T_s + T_{NM}\right)}{g_{ac} T_{NM}} . \tag{6}$$

In order to reduce impact of the receiver system noise temperature drift to increase the measurement

accuracy, a periodic calibration technique is adopted [17], that is, the matched load and the scene are observed alternatively and the corresponding observation output voltage ratio values of K_c and K_x are obtained. Hence, the brightness temperature of observed scene can be determined by:

$$T_x = T_c - \frac{g_{ac}T_{NM}}{g_{dc}}\left(K_c - K_x\right) = T_c - C\left(K_c - K_x\right), \quad (7)$$

where, $C = \frac{g_{ac}T_{NM}}{g_{dc}}$ is the calibration coefficient and it can be determined by liquid nitrogen or tipping calibration. Once the value of C is solved, T_x could be obtained by the above expression.

III. SENSITIVITY ANALYSIS OF THE W-BAND RADIOMETER

As an important parameter for radiometer performance evaluation, the theoretical sensitivity ΔT_{min} which denotes the minimum detectable change in the antenna temperature can be given with the following expression:

$$\Delta T_{\min} = C\sigma K_x, \quad (8)$$

where, σK_x is the standard deviation of K_x defined in Eq. (6). Using the standard propagation of error to obtain σK_x as follows:

$$\sigma K_x = \sqrt{\frac{\sigma V_{DC}^2}{V_{AC}^2} + \frac{V_{DC}^2 \sigma V_{AC}^2}{V_{AC}^4}}, \quad (9)$$

where, σV_{DC} is the standard deviation of DC channel output V_{DC}, and σV_{AC} is the standard deviation of AC channel output V_{AC}. Inserting Eq. (9) into Eq. (8),

$$\Delta T_{\min} = C\sigma K_x = C\frac{V_{DC}}{V_{AC}}\sqrt{\frac{\sigma V_{DC}^2}{V_{DC}^2} + \frac{\sigma V_{AC}^2}{V_{AC}^2}}. \quad (10)$$

It is known from the radiometric principle [18] that the first and the second items in the above square root symbol can be respectively derived as follows:

$$\frac{\sigma V_{DC}^2}{V_{DC}^2} = \frac{\left[\left(\frac{T_s + 2T_{NM}}{\sqrt{B\tau_{dc}/2}}\right)^2 + \left(\frac{T_s}{\sqrt{B\tau_{dc}/2}}\right)^2\right]}{\left(T_s + T_{NM}\right)^2} \approx \frac{4}{B\tau_{dc}}, \quad (11)$$

$$\frac{\sigma V_{AC}^2}{V_{AC}^2} = \frac{\left[\left(\frac{T_s + 2T_{NM}}{\sqrt{B\tau_{ac}/2}}\right)^2 + \left(\frac{T_s}{\sqrt{B\tau_{ac}/2}}\right)^2\right]}{T_{NM}^2} \approx \frac{4\left(T_s + T_{NM}\right)^2}{B\tau_{ac}T_{NM}^2}, \quad (12)$$

where, τ_{dc} and τ_{ac} indicate the integration time of the DC and AC channel respectively, and have the same value of τ due to possessing the identical integrator parameters in this paper. So the obtained radiometer sensitivity is:

$$\Delta T_{\min} = \frac{2\left(T_s + T_{NM}\right)}{\sqrt{B\tau}}\sqrt{1 + \left(1 + \frac{T_s}{T_{NM}}\right)^2}. \quad (13)$$

In the radiometer receiver a simple RC integrator circuit is commonly utilized to smooth the random fluctuation of output signal. However, the integration time of the hardware integrator is fixed and less flexible. So a software digital integrator is generally implemented by averaging digitized samples of the hardware integrator smoothed signal. For a RC integrator with a time constant of τ_{RC}, its pulse response function is:

$$h_{RC}(t) = \begin{cases} 0 & t < 0 \\ \frac{1}{\tau_{RC}}\exp\left(-\frac{t}{\tau_{RC}}\right) & t \geq 0 \end{cases}, \quad (14)$$

and the pulse response function of a digital integrator can be written as:

$$h_{num}(t) = \begin{cases} \frac{1}{\tau_{num}} & -\frac{\tau_{num}}{2} \leq t \leq \frac{\tau_{num}}{2} \\ 0 & else \end{cases}, \quad (15)$$

where, $\tau_{num}=Nt_s$ is the integration time of the digital integrator, N is the number of samples to average, t_s is the sampling interval. Subsequently, the equivalent integration time of the cascaded hardware and software integrators can be determined by combining the convolution computation, the Parseval theorem, and a relationship between the integration time and the power transfer function [19]:

$$\tau = \frac{\tau_{num}^2}{\tau_{num} - \tau_{RC}\left[1 - \exp\left(-\tau_{num}/\tau_{RC}\right)\right]}. \quad (16)$$

Inserting Eq. (16) into Eq. (13), the ultimate expression for the W-band radiometer sensitivity can be rewritten as:

$$\Delta T_{\min} = \frac{2\left(T_s + T_{NM}\right)\sqrt{\tau_{num} - \tau_{RC}\left[1 - \exp\left(-\tau_{num}/\tau_{RC}\right)\right]}}{\tau_{num}\sqrt{B}}\sqrt{1 + \left(1 + \frac{T_s}{T_{NM}}\right)^2}. \quad (17)$$

IV. TIPPING CALIBRATION OF THE W-BAND RADIOMETER

Tipping calibration has been widely applied in the ground based radiometer to determine the calibration coefficient by iterations. For the ideal plane stratified atmosphere, atmospheric radiation transfer theory shows that [20]:

$$T_{sky}(\theta) = T_{bg}e^{-\tau(\theta)} + T_m(\theta)\left(1 - e^{-\tau(\theta)}\right), \quad (18)$$

where, θ is the zenith angle, $T_{sky}(\theta)$ is the sky brightness temperature at the direction of θ, $\tau(\theta)$ is the opacity of total slant path, $T_m(\theta)$ is the atmosphere mean radiative temperature. Define a ratio of opacity between an observation angle θ and the zenith as:

$$m_\theta = \tau(\theta)/\tau(0). \quad (19)$$

For the ideal plane stratified atmosphere, the opacity at the direction of θ is proportional to the opacity at the zenith as described as:

$$\tau(\theta) = \tau(0)\sec\theta. \quad (20)$$

It is seen from Eq. (19) and (20) that $m_\theta = \sec\theta$ for the case of plane stratified atmosphere, and the zenith opacity can be obtained with Eq. (21):

$$\tau(0) = \ln\left(\frac{T_{sky}(0) - T_m(\theta)}{T_{sky}(\theta) - T_m(\theta)}\right) \bullet \frac{1}{m_\theta - 1}, \quad (21)$$

where, $T_{sky}(0)$ and $T_{sky}(\theta)$ are the measured sky brightness temperature values at the directions of 0 and θ. When the opacity is lower, $T_m(\theta)$ can be seen to be constant for different zenith angles, that is, $T_m(\theta) = T_m$. Based on Eq. (7), Eq. (21) can be rewritten as:

$$\tau(0) = \ln\left(\frac{K_{sky}(0) - K_m}{K_{sky}(\theta) - K_m}\right) \bullet \frac{1}{m_\theta - 1}, \quad (22)$$

where, $K_{sky}(0)$ and $K_{sky}(\theta)$ means the acquired voltage ratio defined in Eq. (6) with the sky brightness temperature of $T_{sky}(0)$ and $T_{sky}(\theta)$ respectively. K_m is the voltage ratio associated with mean radiative temperature and can be deducted by K_b which is the voltage ratio of ambient absorber with temperature of T_b described by the following equation:

$$K_m = K_b - (T_b - T_m)/C, \quad (23)$$

where, C is the estimated calibration coefficient. $T_{sky}(0)$ can be determined with the zenith opacity $\tau(0)$ which is calculated by substituting $K_{sky}(0)$、$K_{sky}(\theta)$、K_m and θ into Eq. (22), and hence the calibration coefficient can be rewritten as follows:

$$C = \left(T_b - T_{sky}(0)\right) \Big/ \left(K_b - K_{sky}(0)\right). \quad (24)$$

To improve the accuracy of calibration, the technique of tipping curve is adopted by implementing multiple measurements at different angles. Suppose there is a set of measurement data $\{(a_1, b_1) \cdots, (a_n, b_n)\}$, $a_i = \ln\left(\frac{K_{sky}(0) - K_m}{K_{sky}(\theta_i) - K_m}\right)$, $b_i = m_{\theta_i} - 1$, so the zenith opacity can be calculated using linear regression:

$$y = \tau(0)x + b_\tau, \quad (25)$$

where, $x = m_\theta - 1$, $y = \ln\left(\frac{K_{sky}(0) - K_m}{K_{sky}(\theta) - K_m}\right)$, $\tau(0)$ is the slope of the linear function, b_τ is the intercept which should be close to zero meaning that the fitted line crosses through the origin. The calibration measurement data are invalid unless the correlation coefficient of the regression is greater than a threshold required for accuracy. After renewing the calibration coefficient with $\tau(0)$, the zenith opacity $\tau(0)$ can be also updated and this process is repeated until the intercept converges to zero. It is important to note that the tipping calibration method is based on the ideal plane stratified atmosphere which is met by observations under clear weather conditions.

V. EXPERIMENTAL RESULTS AND ANALYSIS

A. Sensitivity measurement results

For the developed W-band radiometer system, T_R=1340 K, B=2 GHz, C_C=10.6 dB, ENR=15 dB, the integration time of RC integrator is τ_{RC}=50 *ms*, and the sampling interval is t_s=10 *ms*. The relationship between the system equivalent integration time and the number of samples to average is depicted in Fig. 3 according to the Eq. (16).

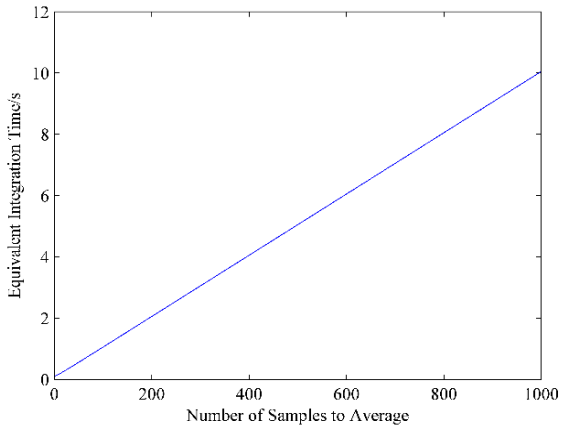

Fig. 3. The relationship between the equivalent integration time and the number of samples.

It can be found from the figure that the system equivalent integration time increases with the numbers of samples almost linearly. Therefore, the integration time of the radiometer can be adjusted by changing the number of samples to average which will lead to a subsequent adjustment of the sensitivity.

To estimate the practical radiometer sensitivity, an ambient absorber with the temperature of 298 K and a liquid nitrogen cooled absorber are observed as a hot and a cold load respectively in the experiment. And the offset parabolic antenna is replaced with a horn antenna for convenience. A group of data with a time length of 10 minutes are acquired for both the hot and cold load observations. And the practical radiometer sensitivity can be calculated as follows:

$$\Delta T_{\min} = \frac{298 - T_{LN2}}{\bar{K}_{Amb} - \bar{K}_{LN2}} \sigma K_x, \quad (26)$$

where, $\bar{K}_{Amb}$ and $\bar{K}_{LN2}$ are the average output voltage ratios for the ambient and cooled absorbers respectively. T_{LN2} is the temperature of absorber soaked in the liquid nitrogen and it can be estimated as [21]:

$$T_{LN2} = 77.36 + 0.011(P - 760), \quad (27)$$

where, P is the atmospheric pressure with the unit of

mmHg.

As presented in Fig. 4, the practical sensitivity is measured under different values of the integration time of 0.1 s, 1 s, and 10 s which are achieved by adjusting the number of samples to average. Also the theoretical sensitivity of the radiometer varied with the integration time is shown by inserting the corresponding parameters into Eq. (17).

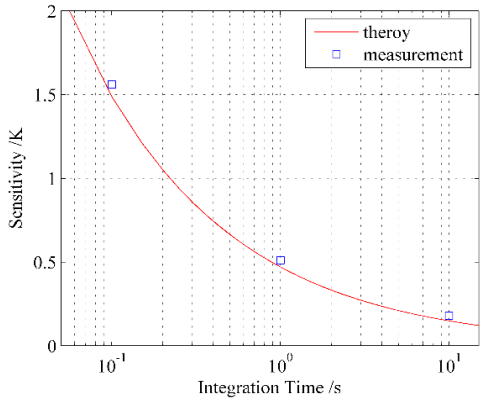

Fig. 4. The radiometer sensitivity with different integration time.

It can be seen that the a sensitivity of 1.56 K is obtained when the integration time is 0.1 s, and its value is reduced to 0.51 K and 0.18 K with a integration time of 1 s and 10 s respectively. Also, the measurement results are in good agreement with the theoretical values.

B. Tipping calibration results

To verify the presented calibration method, calibration experiments of the W-band radiometer were conducted under clear weather conditions in Nanjing, China. The W-band radiometer was placed on the two-dimensional scanner and the antenna pointing zenith angle is set as 0º, 48º, 60º, 66.5 º and 70.5º respectively. The voltage ratios between the DC and AC signal output channels at different observation angles are calculated by the estimated calibration coefficient of C in the first iteration of data processing. Then the zenith opacity is obtained by fitting the calculated data using the least square method and the calibration coefficient of radiometer is renewed consequently. Repeat the above iterative process until the intercept converges to zero.

As the tipping calibration errors might be caused by the pointing angle offset, the mean radiative temperature, the antenna beam width, and the earth curvature, some measures are employed to reduce the calibration errors. For the angular measurement error of scanner is less than 0.05º, the influences of the antenna zenith pointing error on radiometer measurement accuracy could be neglected. To reduce the error caused by the mean radiative temperature T_m, it is calculated by combining the ground temperature, the relative humidity and the meteorological statistics. While for the influence of antenna beam width on calibration error, it could be assessed with the following formula [15]:

$$\delta T_A = \frac{HPBW^2}{16\ln(2)}\left(T_{mr} - T_{bg}\right)e^{-\tau(\theta)}\left[2+\left(2-\tau(\theta)\right)\cot^{-2}(\theta)\right]\tau(\theta), \tag{28}$$

where, $HPBW$ is the antenna half-power beam width in radians. Since the half-power beam width of the radiometer offset parabolic antenna is 0.96º, the maximum of temperature correction within the range of observation angles is less than 0.03 K, and hence the error caused by the antenna beam width is negligible.

In order to reduce the radiometer calibration error caused by the earth curvature, an effective height as in [15] is calculated by utilizing the MMW atmospheric transport model in [22]. Then the ratio of opacity between an observation angle θ and the zenith should be corrected to be:

$$m'_\theta = m_\theta - Hm_\theta(m_\theta{}^2 - 1)/r_e, \tag{29}$$

where H is the effective height, r_e is the radius of the earth.

In the iterative process of calibration, the application of the above correction measures would contribute to a more accurate calibration coefficient. Also, it is essential that the correlation coefficient of the regression needs to meet the accuracy requirement (the minimum value is set to 0.998 in this paper). Two groups of measurement data in the specified angles and the fitted line after 4 iterations are shown in Fig. 5.

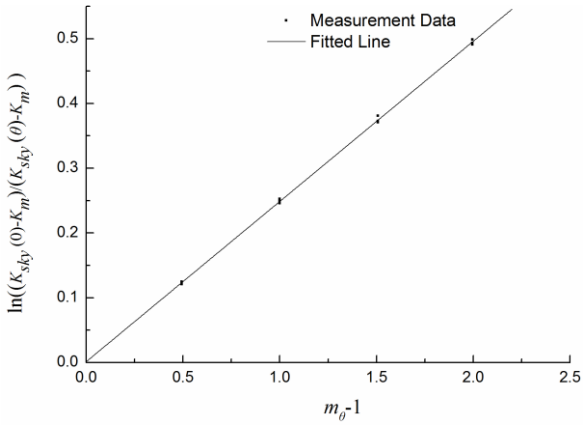

Fig. 5. The measurement data and fitted line of W band radiometer calibration.

The correlation coefficient of the regression is 0.9994, the intercept is 0.001, and the calculated zenith opacity is 0.248. The ultimate radiometer calibration coefficient is estimated to be 586.

C. Evaluation of calibration accuracy

Also to assess the accuracy of the W-band radiometer tipping calibration, a simple liquid nitrogen calibration device is designed. The calibration device is an incubator with wedge-shaped absorber covered inside, and its size is $70cm \times 60cm \times 40cm$. Initially, the radiometer observes the calibration device in the ambient temperature whose value is measured with a high precision thermometer. Then the device filled with liquid nitrogen is observed by the radiometer and the calibration coefficient can be deduced by processing the measurement data. After observations of clear sky at the different observation angles with radiometer, the measurement brightness temperatures are obtained using the calibration coefficient of tipping curve and liquid nitrogen respectively. Define a measurement brightness temperature error ΔT_B:

$$\Delta T_B = T_{B\_TP} - T_{B\_LN2}, \tag{30}$$

where, T_{B_TP} is the measured brightness temperature with the tipping calibration method, T_{B_LN2} is the measured brightness temperature with the liquid nitrogen calibration method. The obtained mean brightness temperature errors at the different directions are shown in Table 1.

Table 1: The mean measurement brightness temperature error at different observation angles

Observation Angle(°)	ΔT_B (K)
0	2.48
30	2.34
45	2.16
60	1.85
70	1.40

As can be seen from the table, the brightness temperature deduced by liquid nitrogen calibration is smaller than that deduced by tipping calibration. And the brightness temperature error between the both reaches the maximum to 2.48 K. Also with the increase of observation angle, the mean measurement brightness temperature error decreases and reaches to about 1.4 K when the observation angle is 70°. The results of this phenomenon are thought to be that real temperature of absorber soaked in liquid nitrogen is higher than the theoretical calculated temperature for the sake of introduced ambient background temperature by radiometer antenna side-lobe and the produced reversed radiation by the liquid nitrogen surface. And then these items lead to a larger radiometer calibration coefficient *C*. However, it is seen from the W-band radiometer system measurement equation as shown in Eq. (7), a larger calibration coefficient will lead to that measured brightness temperature of sky is lower than the actual value. It is proved that the tipping calibration method has a higher accuracy than the liquid nitrogen.

In addition, the matched reference load with ambient temperature is regarded as a standard for the W-band radiometer. When the brightness temperature error between the standard load and the measured object is larger, the error of brightness temperature measurement caused by the calibration coefficient error will be larger due to a larger observation variable of $(K_c\text{-}K_x)$.

Also the calibrated W-band radiometer is placed on the two-dimensional scanner to image a tower with a field of view 30°×14°. The distance between the radiometer and the tower is about 105 m. A picture of the tower is presented in Fig. 6 (a) and the acquired MMW passive image is shown in Fig. 6 (b). The experiment was conducted in a cloudy day with the surface temperature about 310 K. It is shown from the figure that brightness temperature of the scenario varies from 160 K to 300 K where the coldest is the sky, whereas the middle part of tower has the highest temperature. The profile of the tower is clear due to a large contrast between it and the cold sky.

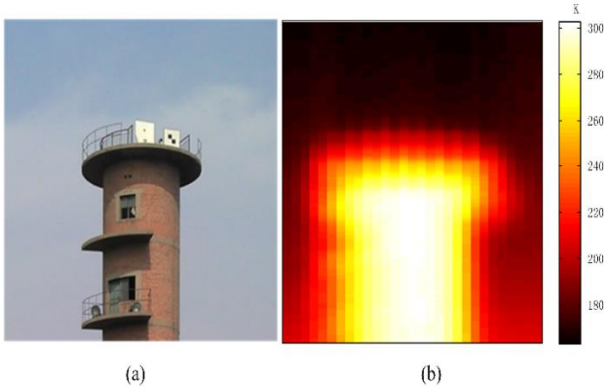

Fig. 6. (a) A picture and (b) a MMW passive image of the tower.

VI CONCLUSION

In this paper, the sensitivity analysis and tipping curve calibration of a developed radiometer for radiometric characterization are presented. The experimental results show that the radiometer sensitivity is 0.51 K with the integration time of 1 s, and the maximum mean measurement brightness temperature difference between tipping curve and liquid nitrogen calibration is 2.48 K for the clear sky and prove the accuracy of tipping calibration. Though the developed radiometer has a mediocre sensitivity due to a high noise figure, the sensitivity of this type of radiometer working at microwave frequencies will be heightened greatly for the noise figure improvements and it will have a great potential for non-contact biomedical sensing. In addition, the tipping calibration presented in this paper will also be promising for the calibration of radiometers in biomedical applications.

ACKNOWLEDGMENT

The authors would like to express their deepest gratitude to Prof. YongXin Guo of National University of Singapore for his insightful comments and suggestions. This work was supported by the National Natural Science Foundation of China (No. 61301213, No. 61501234), and the Natural Science Foundation of Jiangsu Province (No. SBK20130768).

REFERENCES

[1] Q. Bonds, J. Gerig, T. M. Weller, and P. Herzig, "Towards core body temperature measurement via close proximity radiometric sensing," *IEEE Sensors J.*, vol. 12,no. 3,pp. 519-526, 2012.

[2] Z. Popovic, P. Momenroodaki, and R. Scheeler, "Toward wearable wireless thermometers for internal body temperature measurements," *IEEE Commun. Mag.*, vol. 52, no. 10, pp. 118-125, 2014.

[3] F. Bardati and S. Iudicello, "Modeling the visibility of breast malignancy by a microwave radiometer," *IEEE Trans. Biomed. Eng.*, vol. 55, no. 1, pp. 214-221, 2008.

[4] K. Arunachalam, P. R. Stauffer, P. F. Maccarini, S. Jacobsen, and F.Sterzer, "Characterization of a digital microwave radiometry system for noninvasive thermometry using a temperature controlled homogeneous test load," *Phys. Med. Biol.*, vol. 53, no. 14, 2008.

[5] R. Scheeler, E. F. Kuester, and Z. Popovic, "Sensing depth of microwave radiation for Internal body temperature measurement," *IEEE Trans. Antennas Propagat.*, vol. 62, no. 3, pp. 1293-1303, 2014.

[6] C. Liu, Y. X. Guo, and S. Xiao, "Circularly polarized helical antenna for ISM-band ingestible capsule endoscope systems," *IEEE Trans. Antennas Propagat.*, vol. 62, no. 12, pp. 6027-6039, 2014.

[7] S. Yeom, D. S. Lee, Y. S. Jang, M. K. Lee, and S. W. Jung, "Real-time concealed-object detection and recognition with passive millimeter wave imaging," *Opt. Express*, vol. 20, no. 9, pp. 9371-9381, 2012.

[8] B. Quenton, T. Weller, B. Roeder, and P. Herzig, "A total power radiometer (TPR) and measurement test bed for non-contact biomedical sensing applications," *IEEE 10th Annual Wireless and Microwave Technology Conference*, Clearwater, Florida, USA, pp. 1-5, April 2009.

[9] Ø. Klemetsen, Y. Birkelund, S. K. Jacobsen, P. F., Maccarini, and P. R. Stauffer, "Design of medical radiometer front-end for improved performance," *Prog. Electromagn. Res. B.*, vol. 27, pp. 289-306, 2011.

[10] T. Sugiura, H. Hirata, J. W. Hand, J. M. J. Van Leeuwen, and S. Mizushina, "Five-band microwave radiometer system for noninvasive brain temperature measurement in newborn babies: Phantom experiment and confidence interval," *Radio Sci.*, vol. 46, RS0F08, 2011.

[11] J. J. Lynch and R. G. Nagele, "Flicker noise effects in noise adding radiometers," *IEEE Trans. Microw. Theory Techn.*, vol. 59, no. 1, pp. 196-205, 2011.

[12] F. Alimenti, S. Bonafoni, and S. Leone, "A low-cost microwave radiometer for the detection of fire in forest environments," *IEEE Trans. Geosci. Remote Sens.*, vol. 46, no. 9, pp. 2632-2643, 2008.

[13] S. S. Peng, L. Wu, X. H. Ying, and Z. C. Xu, "A receiver in a millimeter wave radiometer for atmosphere remote sensing," *J. Infrared Millim. Terahertz Waves*, vol. 30, no. 3, pp. 259-269, 2009.

[14] S. S. Peng, L. Wu, and X. Q. Li, "Design of 300 mm W-band radiometer offset-feed reflector antenna," *J. Infrared Millim. Terahertz Waves*, vol. 32, no. 6, pp. 545-549, 2013.

[15] Y. Han and E. R. Westwater, "Analysis and improvement of tipping calibration for ground-based microwave radiometers," *IEEE Trans. Geosci. Remote Sens.*, vol. 38, no. 3, pp. 1260-1276, 2000.

[16] J. M. Li, L. X. Guo, L. K. Lin, Y. Y. Zhao, and X. H. Cheng, "A new method of tipping calibration for ground-based microwave radiometer in cloudy atmosphere," *IEEE Trans. Geosci. Remote Sens*., vol. 52, no. 9, pp. 5506-5513, 2014.

[17] M. S. Hersman and A. P. Gene, "Sensitivity of the total power radiometer with periodic absolute calibration," *IEEE Trans. Microw. Theory Techn.*, vol. 29, no. 1, pp. 32-40, 1981.

[18] F. T. Ulaby, R. K. Moore, and A. K. Fung, *Microwave Remote Sensing-Active and Passive, vol. I: Microwave Remote Sensing Fundamentals and Radiometry*, Artech House, Norwood MA, 1981.

[19] L. Gui, K. Chen, L. Lang, and W. Guo, "The sensitivity analysis of full digital compensatory MMW radiometer," *Int. J. Infrared Millimeter Waves*, vol. 28, no. 7, pp. 579-585, 2007.

[20] C. Mätzler, "Ground-based observations of atmospheric radiation at 5, 10, 21, 35, and 94 GHz," *Radio Sci.*, vol. 27, no. 3, pp. 403-415, 1992.

[21] W. N Hardy, "Precision temperature reference for microwave radiometry," *IEEE Trans. Microw. Theory Techn.*, vol. 21, no. 3, pp. 149-150, 1973.

[22] H. J. Liebe, "MPM—An atmospheric millimeter-wave propagation model," *Int. J. Infrared Millimeter Waves*, vol. 10, no. 6, pp. 631-650, 1989.

Li Wu received the B.S., M.S. and Ph.D. degrees all in Electrical Engineering from Nanjing University of Science and Technology (NUST), Nanjing, China, in 2003, 2005 and 2009, respectively. Since 2009, he has been a Lecturer with the School of Electronic and Optical Engineering at NUST. His research interests involve passive imaging, remote sensing, millimeter wave radar system and application.

Shusheng Peng received his B.S. degree from Xiamen University in 1987, M.S. degree from Xi'an Institute of Space Radio Technology in 1990 and Ph.D. degree from Purple Mountain Observatory, Chinese Academy of Sciences in 1995. Since 1997, he has been an Associate Professor and then a Professor with the School of Electronic and Optical Engineering at NUST. His current research interests include millimeter wave detection technology, microwave and millimeter wave radiation measurement technology, the application of embedded system and intelligent sensing and measurement technology.